AD-A034 935 CORPS OF ENGINEERS OMAHA NEBR F/G 8/8
MISSOURI RIVER TEMPERATURE EFFECTS IN THE TRANSITION FROM DUNES--ETC(U)
DEC 76

UNCLASSIFIED NL

1 OF 1
ADA034935

END

DATE
FILMED
3-77

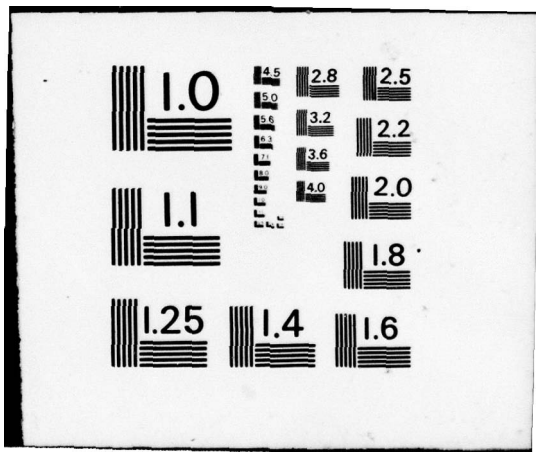
1.0
1.1
1.25
1.4
1.6
1.8
2.0
2.2
2.5
2.8
3.2
3.6
4.0
4.5
5.0
5.6

MISSOURI RIVER

TEMPERATURE EFFECTS IN THE TRANSITION FROM DUNES TO PLANE BED.

PREPARED BY

U.S. GEOLOGICAL SURVEY
IN COOPERATION WITH
U.S. ARMY CORPS OF ENGINEERS

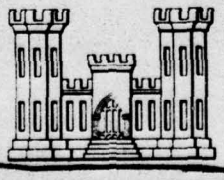

DECEMBER 1976
U. S. ARMY ENGINEER DISTRICT, OMAHA
CORPS OF ENGINEERS
OMAHA, NEBRASKA

M.R.D. Sediment Series

NO. 14

ABSTRACT

Seasonal water-temperature changes influence stage-discharge and depth-discharge relations in rivers and in conveyance channels and navigation channels where water discharge is constant. The major influence is related to changes in bed configuration which accompanies water-temperature changes.

Stability analysis provides a theoretical basis for predicting bed-configuration changes, and using the theoretical relations with one empirical coefficient defined from field data, graphical relations are developed to use as design curves for estimating the velocity and flow depth, given the design unit water discharge, bed material size distribution, water temperature, and channel slope. The design curves are for channels with bed materials from 0.1 to 0.3 mm median diameters, water temperatures for 0 to 30 C, and slopes from 0.00005 to 0.0012.

ACKNOWLEDGMENTS

This report presents the results of a cooperative study undertaken in 1974 by the U.S. Army Corps of Engineers and the U.S. Geological Survey. The assistance of Messrs. Howard C. Christian, Alfred S. Harrison, and Warren W. Mellema of the U.S. Army Corps of Engineers is gratefully acknowledged. Special thanks are due to Professor Frank Engelund and Dr. Jørgen Fredsøe, of the Technical University of Denmark, who developed the theory upon which this report is based and who graciously provided copies of their computer programs for us to use in developing the design curves.

H. Y. Chen
Colorado State University
Fort Collins, Colorado

C. F. Nordin, Jr.
U. S. Geological Survey
Lakewood, Colorado

TABLE OF CONTENTS

LIST OF SYMBOLS

a = complex migration velocity of the bed wave,
a_b = component of bed wave migration velocity affected by bed load,
a_i = imaginary part of a,
a_r = real part of a,
a_s = component of bed wave migration velocity affected by suspended load
a_{bi} = imaginary part of a_b,
a_{si} = imaginary part of a_s,
a_1 and a_2 = coefficients,
C = concentration of the water-sediment mixture,
$\tilde{C}$ = disturbed sediment concentration,
C_o = undisturbed sediment concentration,
C_{bo} = undisturbed sediment concentration at the bed level,
C_1, C_2, C_3, C_4, and c = coefficients,
D = flow depth,
d_b = median diameter of sediment moving as bed load,
d_c = critical particle size,
d_s = median diameter of sediment moving as suspended load,
d_{50} = grain size of which 50 percent is finer by weight,
d_{65} = grain size of which 65 percent is finer by weight,
F = Froude's number,
f = empirical coefficient,
f_1 and f_2 = functions of ξ_y related to the disturbed flow,
g = acceleration of gravity,
h = local height of the sand-bed wave,
h_o = amplitude of the sand-bed wave,
i = imaginary unit,
K = constant,
k = wave number,
k_s = representative sand roughness,
L = wave length of the bed form,
m = porosity of the sand bed,
P_s = water pressure just below the water surface
q = unit-width flow discharge,
q_b = unit-width bed-load discharge
q_s = unit-width suspended-load discharge,
q_t = unit-width bed-material-load discharge,
q_{bo} = undisturbed unit-width bed-load discharge,

q_{so} = undisturbed unit-width suspended-load discharge,
S = bed slope,
S_o = undisturbed bed slope,
s = relative density of sediment,
T = water temperature,
t = time-coordinate,
U = undisturbed flow velocity,
U_{bo} = finite wall slip-velocity,
U_{so} = undisturbed water-surface velocity,
U_{*o} = undisturbed shear velocity,
U'_* = effective shear velocity,
U''_* = shear velocity due to form drag,
u = flow velocity component in x-direction,
$\tilde{U}$ = disturbed flow velocity component in x-direction,
U_* = shear velocity,
V = mean flow velocity,
V_b = total volume per unit bed area of particles transported as bed load,
V_s = total volume per unit bed area of particles transported as suspended load,
v = flow velocity component in y-direction,
$\tilde{v}$ = disturbed flow velocity component in y-direction,
W = fall velocity of a representative sediment particle,
W_c = fall velocity of the critical particle size d_c,
W_s = fall velocity of the representative size of suspended load d_s,
x = space-coordinate in the mean flow direction,
y = vertical space-coordinate,
β = angle related to undisturbed velocity distribution,
ε = eddy coefficient,
η = local height of the water-surface wave,
η_o = amplitude of the water-surface wave,
θ = bed-load transport parameter,
θ_o = undisturbed bed-load transport parameter,
λ = correction factor,
μ = dynamic friction coefficient,
ξ_y = y/D,
ρ = water density,
σ = gradation coefficient, defined by $\frac{1}{2}\,(d_{50}/d_{16} + d_{84}/d_{50})$,
τ = shear stress,
$\tilde{\tau}$ = disturbed shear stress,
τ_o = undisturbed shear stress,
τ' = effective shear stress,
τ'' = shear stress due to form drag,

Ψ = stream function,
$\tilde{\Psi}$ = disturbed stream function,
Ψ_o = undisturbed stream function,
ω = vorticity.

LIST OF FIGURES

INTRODUCTION

Field observations show that for some natural streams and conveyance channels flowing at constant discharge, a change in water temperature alone will promote a drastic change in bed configuration (Colby and Scott, 1965; U.S. Army Corps of Engineers, 1969; Culbertson and others, 1972). Until recently, there was no theoretical basis to identify the mechanism responsible for the changes in bed configurations or to predict the effects of temperature upon bed forms and flow resistance. Despite intense study for many decades the basic hydraulic and transport processes in alluvial channels can be described only in an approximate manner.

A major advance in the theory of alluvial channel flows was the application of linear stability analysis to identify the regions of flow for which the stream bed would be stable; that is, the flow conditions under which a small disturbance of an initially plane bed would be dampened. Early theories of Exner (1925) and Polya (1937) predicted instability of the bed, but no stable regions. Anderson (1953) first pointed out the importance of the strong interaction between water surface and bed waves for antidunes, bed and water surface configurations that had been documented many years earlier by Pierce (1916) and Gilbert (1914). However, it was Kennedy (1961, 1963) who first put forth a comprehensive theory to account for dunes, a plane bed, and antidunes by means of linear stability analysis. Kennedy used a potential flow model with an empirical relation between flow velocity and sediment transport; in later studies the basic theory was extended to the formation of ripples in closed conduits (Kennedy, 1964) and to ripples formed in oscillatory flows (Kennedy and Falcon, 1965). An excellent review article summarizes the basic theory and its application (Kennedy, 1969).

Many others have contributed to the stability approach (Reynolds, 1965; Gradowczyk, 1968; Smith, 1970; Engelund and Hansen, 1966; Hayashi, 1970; Engelund, 1970), and it is well established that stability analysis can explain, at least to a first approximation, the essential features of the observed data on bed configurations in alluvial channels.

The earlier stability analyses of Kennedy (1963) and Reynolds (1965) were based on potential flow models and so were not capable of including any dynamic effects. Engelund (1970) introduced a real fluid model that provided a more realistic description of the dynamic forces, the flow, and the coupled sediment transport. However, all of the linear stability analyses have in common two major shortcomings. First, because of the linearity, only first order effects are considered, and this can serve to identify only the initial instabilities. The equilibrium height and final wavelength to which dunes can grow cannot be predicted by linear methods, nor can the flow separation or nonsymmetry of the bed forms be described. Second, although the stability analyses have provided a great deal of insight into the mechanism of

flow in alluvial channels, they have not led to any practical advances in design of stable channels or in prediction of bed forms and flow resistance. If one knows all the flow and sediment variables required for the stability analyses, all the essential features of the flow required for a practical design problem are known.

Recently, Engelund and Fredsøe (1974) introduced some important new concepts into stability analysis. They began with the vorticity transport equation to describe the flow, following the basic model proposed by Engelund (1970), and they proposed that the stability of the bed, described by the imaginary part of the bed-wave migration velocity, was dependent upon the ratio of suspended load to bed load. A temperature-dependent transport relation in which it is assumed that all particles smaller than a critical size will enter into suspension was introduced, and because the critical size depends on the ratio of particle-fall velocity to shear velocity, the analysis predicts very well the transition from dune to plane bed with decreasing water temperature.

The purpose of this report is to extend the analysis presented by Engelund and Fredsøe (1974) to a greater range of conditions so that stability boundaries between dunes and a plane bed can be identified and presented graphically as aids in practical channel-design problems. In the following section, some of the basic elements of stability analysis as developed by Engelund and Fredsøe (1974) are presented. This is followed by a summary of the results of the stability analysis, presented graphically, and finally, it is shown how an extension of the basic equations can provide an estimate of mean velocity and flow depth if the channel width, design discharge, particles size and water temperature are known. A numerical example is given in the appendix.

STABILITY ANALYSIS

1. General Approach

The usual approach to fluid-stability analysis is to introduce a small perturbation to the flow and to investigate how the amplitude of the perturbation increases or decreases with time. Usually, the perturbation takes the form of a sinusoid so that its amplitude can be described in complex form. If the imaginary part grows with times, the flow is unstable, while if the imaginary part is dampened, the flow is stable.

For flow over a sand bed, the stability analysis is complicated because the flow equation and the sediment transport must be coupled and because the model must account both for the dune case where the water-surface and bed waves are out of phase and for the antidune case when the bed and water-surface waves are in phase. The migration of the bed forms must be included and transport both of bed load and suspended load has to be considered.

In the following section, the stability theory derived by Engelund and Fredsøe (1974), that accounts for all these factors is outlined. The discussion here follows very closely the original work of Engelund and Fredsøe (1974), where a complete derivation of the stability theory is given.

2. Summary of the Theory

(1) Flow equations

The perturbed flow for two dimensional flow over a slightly sinusoidal bed may be described by the vorticity transport equation (Engelund, 1970)

$$\frac{d\omega}{dt} = \varepsilon \nabla^2 \omega \tag{1}$$

in which ε is the eddy viscosity. The vorticity ω is defined by

$$2\omega = \frac{\partial v}{\partial x} - \frac{\partial u}{\partial y} \tag{2}$$

where x is a coordinate in the mean flow direction, y is a vertical coordinate, and u and v are the velocity components in the x and y directions, respectively. The stream function ψ for the flow is defined by

$$u = -\frac{\partial \psi}{\partial y}$$

and (3)

$$v = \frac{\partial \psi}{\partial x}$$

If Eqs. (2) and (3) are substituted into the vorticity transport equation, we get

$$-\frac{\partial \psi}{\partial y}\frac{\partial(\nabla^2\psi)}{\partial x} + \frac{\partial \psi}{\partial x}\frac{\partial(\nabla^2\psi)}{\partial y} + \frac{\partial(\nabla^2\psi)}{\partial t} = \varepsilon \nabla^4 \psi \tag{4}$$

Next, the distribution of the suspended load in a nonuniform flow is described by a local continuity equation expressing the equilibrium between settling, diffusion and convection of sediment

$$\frac{dC}{dt} = W \frac{\partial C}{\partial y} + \varepsilon \nabla^2 C \tag{5}$$

where C is the concentration of the water-sediment mixture and W is the fall velocity of a representative sediment particle. When the uniform flow is perturbed, it is assumed that the perturbation of the flow is periodic and is described by the following relations (Engelund and Fredsøe, 1974),

$$h = h_o exp \left\{ ikD \left(\frac{x}{D} - \frac{a}{D} t \right) \right\} \tag{6}$$

$$\eta = \eta_o exp \left\{ ikD \left(\frac{x}{D} - \frac{a}{D} t \right) \right\} \tag{7}$$

$$a = a_r + i\, a_i \tag{8}$$

$$\psi = \psi_o + \tilde{\psi} \tag{9}$$

$$\tilde{\psi} = U_{bo} h_o f_1\left(\frac{y}{D}\right) exp \left\{ ikD \left(\frac{x}{D} - \frac{a}{D} t \right) \right\} \tag{10}$$

$$C = C_o + \tilde{C} \tag{11}$$

$$\tilde{C} = \frac{h_o}{D} f_2\left(\frac{y}{D}\right) exp \left\{ ikD \left(\frac{x}{D} - \frac{a}{D} t \right) \right\} \tag{12}$$

in which h is the local height of the sand-bed wave (see definition sketch, Fig. 1), h_o is the amplitude of the sand-bed wave, kD is the dimensionless wave number with $k = 2\pi/L$, L is the wave length, a is the complex migration velocity of the bed waves, η is the local height of water-surface wave, ψ_o is the undisturbed stream function, $\tilde{\psi}$ is the disturbed stream function, U_{bo} is the finite wall slip-velocity, C_o

and $\tilde{C}$ are the undisturbed and the disturbed sediment concentrations, and $f_1(\frac{y}{D})$ and $f_2(\frac{y}{D})$ are unknown functions to be found by solving the vorticity transport equation (4) and sediment continuity equation (5).

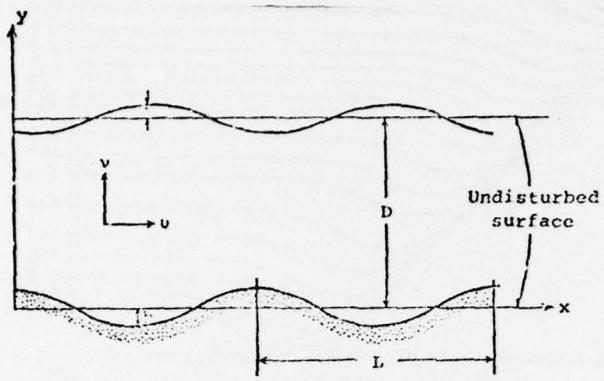

Figure 1.--Definition sketch.

To solve Eqs. (4) and (5), the undisturbed velocity and concentration distributions are required. The undisturbed velocity profile can be described by the parabolic velocity distribution in the major part of the flow (outside the viscous sublayer) from integration of the flow equation. Assuming a constant value of the eddy viscosity ε, the undisturbed velocity profile is described by

$$U = U_{so} + \frac{D\, U_{*o}}{\varepsilon}\left[\frac{y}{D} - \frac{1}{2}\left(\frac{y}{D}\right)^2 - \frac{1}{2}\right] \tag{13}$$

where U_{so} and U_{*o} are the undisturbed surface velocity and shear velocity, respectively, and ε is given by (Hinze, 1959)

$$\varepsilon = 0.077\, U_{*o} D \tag{14}$$

The quantity U_{*o} is actually the effective shear velocity U_*' over a plane bed and is found from a graphical solution of the Einstein-Barbarossa equation (Fig. 2, from Vanoni and Brooks, 1957). In order to obtain a simple analytical solution, the equation of a parabola (13) is replaced by a cosine given by the expression

$$U = U_{so} \cos\left[\beta\left(1 - \frac{y}{D}\right)\right] \tag{15}$$

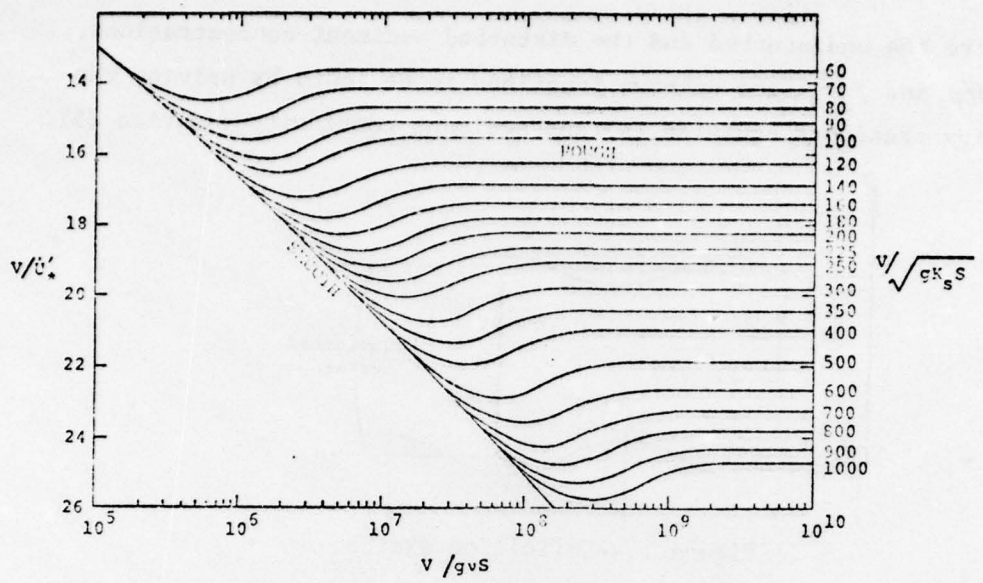

Figure 2a.--Curves for graphical solution of Einstein-Barbarossa equations for determination of r' and r".

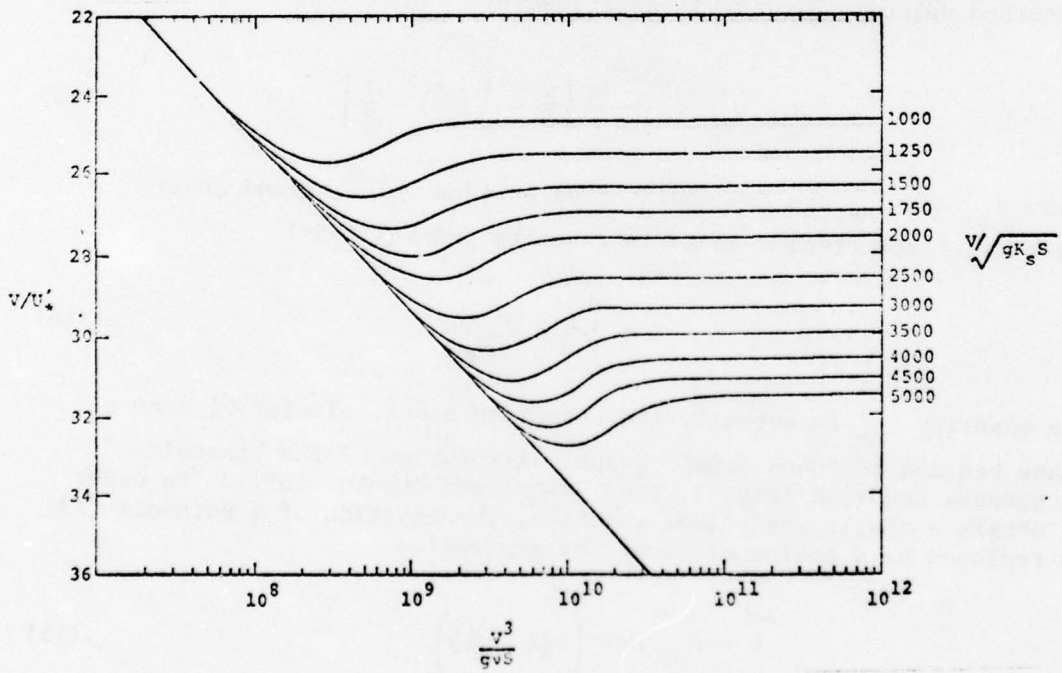

Figure 2b.--Curves for graphical solution of Einstein-Barbarossa equations for determination of r' and r".

with $\beta^2 = 14 \frac{U_{*o}}{U_{BO}}$ to approximate the parabola. A finite wall slip velocity U_{bo} must be introduced with the assumption of constant eddy viscosity (Engelund, 1970)

$$U_{bo} = U_{so} \cos \beta \tag{16}$$

which is found by matching the velocity profile outside the viscous sublayer with a known logarithmic velocity profile near the bottom. For a hydraulically rough bed, the matching condition is

$$\frac{U_{bo}}{U_{*o}} = 1.9 + 2.45 \ln \frac{D}{k_s} = K \tag{17}$$

where K is a constant and k_x is the representative sand roughness and is taken to equal 2.5 d_b with d_b the mean diameter of the bed material.

The undisturbed concentration C_o can be found by solving Eq. (5) in the steady uniform flow as

$$C_o = C_{bo} \exp(-\frac{Wy}{\varepsilon}) \tag{18}$$

where C_{bo} is a sediment concentration at the bed level.

When Eqs. (9) through (12) are substituted into Eqs. (4) and (5), we obtain the following pair of ordinary differential equations in f_1 and f_2 on the assumptions that $h_o << D$ and $a << U$:

$$f_1'' - \left[(kD)^2 + \frac{U''}{U}\right] f_1 = \frac{\varepsilon}{ikD^2U} f_1'''' \tag{19}$$

and

$$f_2'' + \frac{WD}{\varepsilon} f_2' - \left[(kD)^2 + ikD \frac{UD}{\varepsilon}\right] f_2 = ikD \frac{U_{bo}D}{\varepsilon} f_1 \frac{dC_o}{d\xi_y} \tag{20}$$

where $\xi_y = y/D$ and all differentiations are made with respect to ξ_y.

Analytical solutions to Eqs. (19) and (20) are

$$f_1(\xi_y) = C_1 \exp\left[\xi_y \sqrt{(KD)^2 - \beta^2}\right] + C_2 \exp\left[-\xi_y \sqrt{(KD)^2 - \beta^2}\right]$$

$$+ C_3 \exp\left[-\xi_y \sqrt{ikD \frac{U_{bo}D}{\varepsilon}}\right] + C_4 \exp\left[\xi_y \sqrt{ikD \frac{U_{so}D}{\varepsilon}}\right] \qquad (21)$$

and

$$f_2(\xi_y) = \Bigg[a_1 \exp\left[\xi_y\left(-\frac{WD}{2\varepsilon} - \sqrt{\left(\frac{WD}{2\varepsilon}\right)^2 + (kD)^2 + ikD\frac{U_{bo}D}{\varepsilon}}\right)\right]$$

$$+ a_2 \exp\left[\xi_y\left(-\frac{WD}{2\varepsilon} + \sqrt{\left(\frac{WD}{2\varepsilon}\right) + (kD)^2 + ikD\frac{U_{so}D}{\varepsilon}}\right)\right]$$

$$- ikD\frac{U_{bo}D}{\varepsilon}\frac{WD}{\varepsilon}\Bigg\{\frac{C_1 \exp\left[\xi_y\left(\sqrt{(kD)^2 - \beta^2} - \frac{WD}{\varepsilon}\right)\right]}{-\beta^2 - \frac{WD}{\varepsilon}\sqrt{(kD)^2 - \beta^2} - ikD\frac{U_{bo}D}{\varepsilon}}$$

$$+ \frac{C_2 \exp\left[\xi_y\left(-\sqrt{(kD)^2 - \beta^2} - \frac{WD}{\varepsilon}\right)\right]}{-\beta^2 + \frac{WD}{\varepsilon}\sqrt{(kD)^2 - \beta^2} - ikD\frac{U_{bo}D}{\varepsilon}}$$

$$+ \frac{C_3 \exp\left[\xi_y\left(-\sqrt{ikD\frac{U_{bo}D}{\varepsilon}} - \frac{WD}{\varepsilon}\right)\right]}{\sqrt{ikD\frac{U_{bo}D}{\varepsilon}\frac{WD}{\varepsilon}} - (kD)^2}$$

$$+ \frac{C_4 \exp\left[\xi_y\left(\sqrt{ikD\frac{U_{so}D}{\varepsilon}} - \frac{WD}{\varepsilon}\right)\right]}{-\sqrt{ikD\frac{U_{so}D}{\varepsilon}\frac{WD}{\varepsilon}} - (kD)^2}\Bigg\}\Bigg] C_{bo} \qquad (22)$$

The coefficients C_1, C_2, C_3, C_4, a_1, and a_2 in Eqs. (21) and (22) can be found from six boundary conditions described in Sec. 2-(2). Once the functions f_1 and f_2 are determined, the migration velocity of bed waves is obtained by solving the sediment continuity equation

$$\frac{\partial q_T}{\partial x} = -\ (1 - m)\ \frac{\partial h}{\partial t} \tag{23}$$

or in another form

$$a\ (1 - m)\ \frac{\partial h}{\partial x} = \frac{\partial q_T}{\partial x} \tag{24}$$

where m is the porosity of the sand bed and q_T is the total bed material load which is the sum of the bed load q_b and the suspended load q_s. The value of the imaginary part a_i of the migration velocity determines the stability of the sand bed. Eq. (6) can be written as

$$h = h_o\ exp\ (ka_i t)\ exp\ \left[ikD\left(\frac{x}{D} - \frac{a_r}{D}\ t\right)\right] \tag{25}$$

where ka_i is called the amplification factor. If a_i is found to be positive, the sand bed will be unstable because the amplitude of the perturbation will increase in time. Correspondingly, the bed will be stable if $a_i < 0$. Furthermore, the real part a_r determines the migration velocity of the bed wave in the flow direction as well as the type of the bed form. If $a_r > 0$, the bed wave migrates downstream and the bed is about 180^o out of phase with the water surface. The sand bed has the characteristics of dunes. In the case of antidunes, bed and water surface are approximately in phase and $a_r < 0$.

(2) Boundary conditions

To obtain the four coefficients C_1, C_2, C_3, and C_4 in Eq. (21), the following four conditions are employed:

(i) The kinematical condition at the sand bed is

$$\frac{dh}{dt} = \frac{\partial h}{\partial t} + u\ \frac{\partial h}{\partial x} = v \tag{26}$$

at $\xi_y = h/D$. When eqs. (3), (6), (9) and (10) are introduced, Eq. (26) is reduced to

$$f_1(0) = 1 \tag{27}$$

assuming $a/U_b \ll 1$ and $h/D \ll 1$.

(ii) The same kinematical condition at the surface yields

$$f_1(1) = \frac{U_{so}}{U_{bo}} \frac{\eta_o}{h_o} \tag{28}$$

and the shear stress

$$\frac{\tau}{\rho} = \varepsilon \left(\frac{\partial u}{\partial y} + \frac{\partial v}{\partial x}\right) = U_*^2 \tag{29}$$

must vanish at the free surface. Eqs. (28) and (29) lead to the second boundary condition

$$f_1''(1) + f_1(1) \left[(kD)^2 + \frac{DU_{*o}}{\varepsilon U_{so}}\right] = 0 \tag{30}$$

(iii) The normal stress must vanish at the free surface. To a first order approximation, this is expressed as

$$\frac{P_s}{\rho} = 2 \varepsilon \frac{\partial v}{\partial y} \tag{31}$$

The surface tension is neglected and P_s is the water pressure just below the surface. To eliminate P_s from Eq. (31), the equation of motion at $\xi_y = 1$ is considered

$$\frac{du}{dt} = - \frac{\partial}{\partial x} \left(g\eta + \frac{P_s}{\rho}\right) + \varepsilon \nabla^2 u + gS_o \tag{32}$$

in which S_o is the mean slope of the channel equal to the slope of the undisturbed water surface. S_o must satisfy the relation

$$\varepsilon \frac{\partial^2 U}{\partial y^2} + g S_o = 0 \tag{33}$$

Based on Eqs. (31), (32), and (33), the boundary condition becomes

$$f_1'''(1) + \left[-ikD \frac{U_{so} D}{\varepsilon} - 3(kD)^2\right] f_1'(1) + \frac{qD}{\varepsilon U_{so}} ikD f_1(1) = 0 \tag{34}$$

(iv) The condition (17) is also assumed to be valid in the perturbed flow, i.e.

$$\frac{U_b}{U_*} = K \tag{34a}$$

at $\xi_y = h/D$. Determining the local value of U_* by Eq. (29), the linear form of Eq. (34) is

$$f_1''(0) - \frac{2U_{bo} D}{K^2 \varepsilon} f_1'(0) + (kD)^2 f_1(0) = \frac{U''}{U} - \frac{2U_{bo} D}{K^2 \varepsilon} \frac{(U')\xi_y}{U_{bo}} = 0 \tag{35}$$

with all differentiations being with respect to ξ_y.

Two boundary conditions are required to obtain the two constants a_1 and a_2 in Eq. (22).

(k) The relation between the bed concentration C_b and the local value of the shear stress is assumed to follow

$$\frac{C_b}{C_{bo}} = \left(\frac{\tau}{\tau_o}\right)^{3/2} \tag{36}$$

where τ_o is the undisturbed bed shear stress. After the substitution, the linearized form turns out to be

$$\tilde{C} + h \frac{dC_o}{dy} = \frac{3C_{bo}}{U_{bo}} \left(- \frac{\partial \tilde{\Psi}}{\partial y} + h \frac{dU}{dy} \right)$$

or

$$f_2(0) = 3C_{bo} \left[\frac{WD}{3\varepsilon} - f_1'(0) + \beta \tan \beta \right] \tag{37}$$

(ii) At the water surface, the vertical sediment flux must vanish

$$\varepsilon \frac{\partial \tilde{C}}{\partial y} + W\tilde{C} = 0$$

Substitution of Eq. (12) for $\tilde{C}$ into the above equation yields

$$f_2'(1) + \frac{WD}{\varepsilon} f_2(1) = 0 \tag{38}$$

(3) Sediment transport

To determine the migration velocity of the bed wave from Eq. (24), knowledge of sediment transport is needed. Sediment transport rates are affected by a large number of factors, and there is still no method available at present for accurately estimating the sediment discharge under different flow conditions. In this analysis, the bed load transport rate q_b is assumed to follow the Meyer-Peter formula

$$\Phi_b = \frac{q_b}{\sqrt{(s-1)g\, d_b^3}} = 8(\theta - 0.047)^{3/2} \tag{39}$$

where s is the relative density of the sediment, g is the acceleration of gravity, d_b is the mean diameter of the grain moving as bed load, and θ is a parameter representing the ratio between the effective shear stress at the bed and the stabilizing forces on a sediment particle in the bed

$$\theta = \frac{\tau'}{\rho(s-1)g\, d_b} + \mu S \tag{40}$$

where τ' is the effective shear stress, S is the bed slope and μ is a dynamic friction coefficient estimated to be 0.1. The ratio between disturbed and undisturbed bed load transport rates is then

$$\frac{q_b}{q_{bo}} = \frac{(\theta-0.047)^{3/2}}{(\theta_o-0.047)^{3/2}} \tag{41}$$

where

$$\theta_o = \frac{U_{*o}^2}{(s-1)g\ d_b} + \mu S_o$$

in which S_o is the undisturbed plane bed slope.

The rate of suspended sediment transport q_s is found from

$$q_s = \int_h^{D+\eta} uCdy \simeq q_{so} - U_{bo}C_{bo}h + \int_o^1 \left[(-U_{bo})\ f_1'(\xi_y)\ hC_o + Uhf_2(\xi_y)\right] d\xi_y \tag{42}$$

where

$$q_{so} = D\int_o^1 UC_o d\xi_y$$

is the suspended load transport rate over an undisturbed flat bed.

The quantities q_{bo} and q_{so} can be estimated from Eqs. (39) and (42) provided d_b and C_{bo} are known. These two quantities can be evaluated based on the following two assumptions:

(i) Sediment particles finer than a certain critical size all enter into suspension while larger particles move as bed load. A preliminary criterion for determining the critical particle size was suggested by Engelund (1973)

$$W_c = 0.8\ U_*' \tag{43}$$

Once the critical settling velocity W_c and the corresponding size d_c are determined, the median size of the bed load can be estimated from the bed material size distribution.

(ii) No segregation takes place so the moving particles keep the original composition of the bed material. This assumption states that

$$\frac{V_b}{V_s} = \frac{\text{(total volume of particles transported as bed load)}}{\text{(total volume of particles transported as suspended load)}}$$

$$= \frac{\text{Percent bed material coarser than } d_c}{\text{Percent bed material finer than } d_c} \qquad (44)$$

where in a unit area

$$V_b = 0.5 d_b \ ,$$

and

$$V_s = \int_d^D C_o \, dy \simeq D \, C_{bo} \left[\frac{W_s D}{\varepsilon}\right]^{-1} \ ,$$

W_s is the fall velocity of the representative size of suspended load d_s and percent loads are obtained from assumption (i). Eq. (44) yields the value of C_{bo}.

It is interesting to note the temperature effects on the sediment transport rates. The primary effect of temperature is its large influence on the viscosity of the fluid and on the fall velocity of sand particles in suspension. A decrease in the water temperature increases the fluid viscosity and decreases the fall velocity of suspended particles. Based on assumption (i), the decrease in temperature increases the critical size and thus increases the percent suspended load of the total load. Then from assumption (ii), this will increase the value of C_{bo} and will cause the concentration distribution to be more uniform. An example of temperature effects on the sediment transport rates calculated from Eqs. (39) and (42) is shown in Fig. 3. The decrease in temperature significantly increases the suspended load discharge but has only slight effect on the bed load. In this example, the velocity and the depth are assumed unchanged with temperature. However, if the flow conditions are close to the transition zone, the temperature changes may change the bed form and its resistance to flow. In this case, the decrease in temperature will increase the velocity and decrease the depth for a given flow discharge, and therefore tremendously increase the ability of the stream to carry the sediment load.

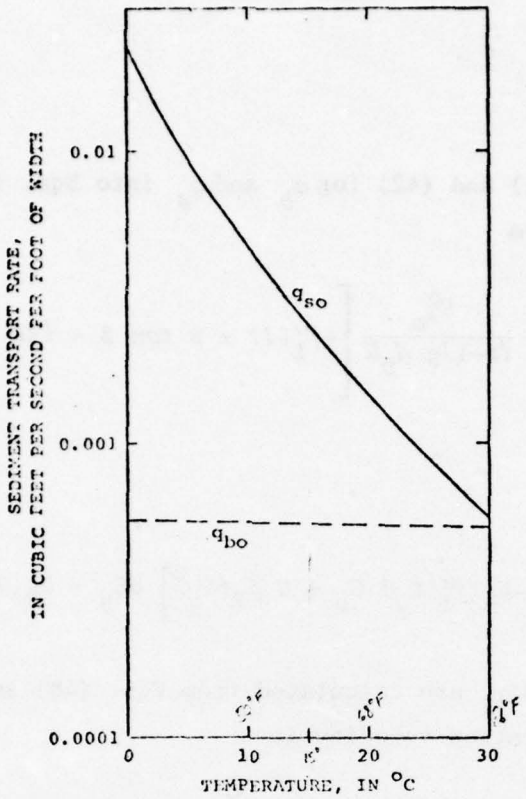

Figure 3.--Temperature effects on the sediment transport rates (q = 50 cfs/ft, d_m = 0.21 mm, σ = 1.23, S = 0.00015 and F = 0.25)

(4) Migration Velocity

The migration velocity determines the stability of the bed and also the form of bed roughness as stated in Sec. 2-(1). Its value can be determined from the sediment continuity equation (24). If the part of the total sediment discharge carried in suspension is converted to an equivilant bed migration velocity; Eq. (24) can be written as

$$(a_b + a_s)\ (1-m)\ \frac{\partial h}{\partial x} = \frac{\partial q_b}{\partial x} + \frac{\partial q_s}{\partial x} \tag{45}$$

where a_b and a_s are components of migration velocity affected by bed load and suspended load transport rates, respectively. Eq. (45) can be written correspondingly as

$$a_b\ (1-m)\ \frac{\partial h}{\partial x} = \frac{\partial q_b}{\partial x} \tag{46}$$

and

$$a_s (1-m)\ \frac{\partial h}{\partial x} = \frac{\partial q_s}{\partial x} \tag{47}$$

Substituting Eqs. (41) and (42) for a_b and q_s into Eqs. (46) and (47) yields the linear form

$$a_b = \frac{3}{1-m} \frac{q_{bo}}{(\theta_o - 0.047)} \frac{U_{*o}^2}{(s-1)g\, d_b D} \left[-f_1'(0) + \beta \tan \beta - ikD \frac{\mu}{2} \frac{g d_b (s-1)}{U_{*o}^2} \right] \tag{48}$$

and

$$a_s = \frac{1}{1-m} \left\{ \int_o^1 \left[-U_{bo} f_1'(\xi_y)\, C_o + U f_2(\xi_y) \right] d\xi_y - U_{bo} C_{bo} \right\} \tag{49}$$

When values of a_b and a_s are calculated from Eqs. (48) and (49), the equivalent total migration velocity is

$$a = a_b + a_s \tag{50}$$

The imaginary part becomes

$$a_i = a_{bi} + a_{si} \tag{51}$$

The values of a_i strongly depend on the ratio between bed load and suspended load. In Fig. 4, an example of the quantities a_{bi} and a_{si} is presented. The figure shows that $a_{si} < 0$ and $a_{bi} > 0$ when the Froude number is less than 0.8. This indicates that in the lower flow regime the suspended load stabilizes the bed while the bed load reverses the effect. Both a_{bi} and $-a_{si}$ increase with an increase in Froude number. However, when the Froude number is larger than a certain value, $-a_{si}$ increases much faster than a_{bi}. Hence, when the Froude number is low, a_i is positive indicating bed instability with bed forms of dunes, while for high Froude number, a_i becomes negative indicating bed stability (flat beds).

In Fig. 4, the temperature effects on a_{bi} and a_{si} also are shown. A decrease in temperature increases both a_{bi} and $-a_{si}$. Nevertheless,

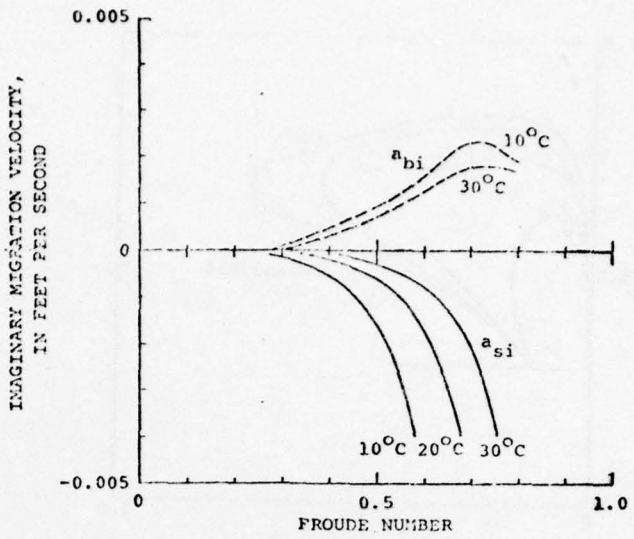

Figure 4.--Temperature effects on the imaginery migration velocity of bed wave (D = 0.33 ft, d_m = 0.21 mm, σ = 1.23, k_D = .21)

the increase in $-a_{si}$ is larger because of the large temperature effect on the suspended load as shown in Fig. 3. This indicates that dunes disappear at lower Froude numbers when the temperature is low.

3. Results of the Stability Analysis

As shown in Fig. 4, for a given wave number kD, depth D, median size of bed material d_{50}, gradation coefficient of sediment size distribution σ and water temperature T, the bed may be stable or unstable depending on the flow velocity. When kD is plotted against Froude number F keeping other variables unchanged, a set of transition curves distinguishing dunes and plane bed is obtained as shown in Fig. 5. In the figure, the instability of the lower flow regime disappears at a Froude number about 0.84 and temperature 30° Celsius. As pointed out in Sec. 2-(4), this transition between dunes and plane bed depends on the ratio between bed load and suspended load. Because temperature has significant effects on this ratio, the decrease in water temperature lowers the stability limits of the transition line and thus may remove dunes from the sand bed. From the figure, it is concluded that the transition from dunes to plane bed always takes place at very large wavelengths.

Figure 6 shows more specifically the temperature effects on bed stability. The curves represent the upper limit for the existence of dunes as functions of D, T, d_{50}, σ and mean flow velocity V. For a given depth and velocity if the temperature decreases to a certain value the dunes disappear. For example, when D = 10 ft and V = 6.5 fps, if T is less than 30° Celsius, the bed form changes from dunes toward a plane bed. At a still lower temperature, the change from

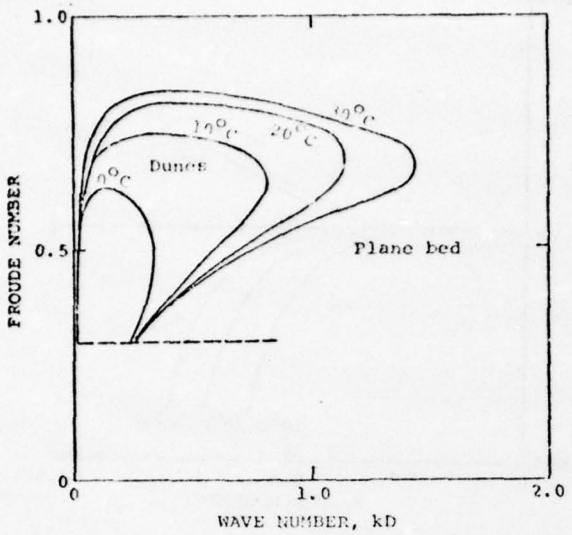

Figure 5.--Temperature effects on the instability regime ($D = 0.33$ ft, $d_{50} = 0.3$ mm, $\sigma = 1.23$)

dunes to plane bed occurs at a lower velocity. However, if the flow conditions are far below the transition zone, the temperature effect is not significant.

The most obvious example of temperature effect is that reported for the Missouri River (U.S. Army Corps of Engineers, 1969), where a decrease in temperature during the autumn first causes a stretching of the dunes and finally smoothes out the bed so that it becomes completely plane. When Missouri River data (see Table 1) are plotted on Fig. 6, they fall mostly between the transition curves of $T = 20°$ and 10° Celsius. Then, as indicated in this figure, the decrease in temperature lowers the critical curve, changes the bed form from dunes to plane bed, decreases the depth and increases the velocity.

FLOW RESISTANCE

When the flow parameters nearly satisfy the conditions for transition between dunes and plane bed, the effects of temperature on flow characteristics become significant. The decrease in temperature smoothes out the sand bed and therefore reduces its resistance to flow. This reduction in flow resistance increases the flow velocity and decreases the depth for a given unit-width flow discharge as shown in Fig. 6. Nevertheless, the amount of change cannot be evaluated from Fig. 6. An attempt to predict the temperature effects on resistance to flow is initiated here based on stability theory.

1. Theoretical Analysis

The shear stress can be related to the velocity gradient as

$$\frac{\tau}{\rho} = \varepsilon\left(\frac{\partial u}{\partial y} + \frac{\partial v}{\partial x}\right) \tag{52}$$

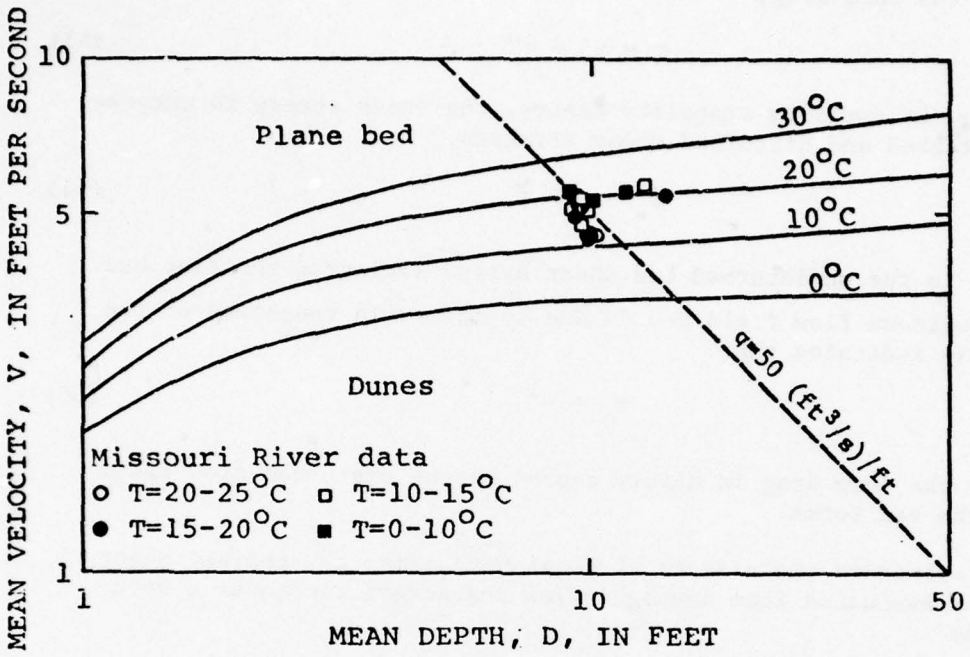

Figure 6.--Temperature effects on the upper limit to existence of dunes

(d_m = 0.21 mm, σ = 1.23)

In practice, the bed shear stress is commonly composed of the surface drag and the form drag,

$$\tau \simeq \tau' + \tau'' \tag{53}$$

Similarly, by applying stability theory, the shear stress is composed of undisturbed and disturbed shear stresses,

$$\tau \simeq \tau_o + \tilde{\tau} \tag{54}$$

where τ_o is the undisturbed bed shear stress acting on the flat bed under a uniform flow field and is due to the grain roughness of the bed. This indicates that

$$\tau_o \simeq \tau' \tag{55}$$

and that the form drag is mainly caused by the disturbed flow field due to the bed forms.

To eliminate the effects of local nonuniformity, the bed shear stress is evaluated from averaged flow characteristics over a wave length as

$$\bar{\tau} = \tau_o + \lambda \left[\frac{2}{L/4} \int_o^{L/4} \tilde{\tau}\, dx \right] \tag{56}$$

where L is the bed wave length, and λ is a correction factor to relate the energy dissipation due to form roughness to the disturbed flow field on the bed. The disturbed shear stress is averaged over a quarter of the wave length and then multiplied by 2 to account for the flow disturbance caused by the bed wave of amplitude $(2h_o)$. Comparing Eqs. (53) and (54) leads to

$$\tau'' = \lambda \left(\frac{8}{L} \int_o^{L/4} \tilde{\tau}\, dx \right) \tag{57}$$

Applying the stability theory, the quantity τ can be expressed by

$$\frac{\tilde{\tau}}{\rho} = \varepsilon \left(\frac{\partial \tilde{u}}{\partial y} + \frac{\partial \tilde{v}}{\partial x} \right)$$

$$= \varepsilon \left(- \frac{\partial^2 \tilde{\psi}}{\partial y^2} + \frac{\partial^2 \tilde{\psi}}{\partial x^2} \right) \tag{58}$$

Substituting Eq. (10) for $\tilde{\Psi}$ into Eq. (58), the disturbed shear stress in steady nonuniform flow is

$$\frac{\tilde{\tau}}{\rho} = -2U_{*o}^2 \frac{h_o}{D}\left[f''(0) - \beta \tan \beta\right] \exp\left(i2\pi \frac{x}{L}\right) \tag{59}$$

This equation can be rewritten with the aid of Eq. (48) as

$$\frac{\tau}{\rho} = \frac{1}{12}\frac{h_o(1-m)}{d_b}\sqrt{\frac{(s-1)g\ d_b}{(\theta_o-0.047)}}\left[a_b + \frac{1.2ikD}{(1-m)D}\sqrt{(\theta_o-0.047)(s-1)g\ d_b^3}\right]\exp\left(i2\pi\frac{x}{L}\right) \tag{60}$$

Substituting Eq. (60) into Eq. (57) for τ and then integrating Eq. (57), the real part of the resulting relation equals the form drag, that is

$$\frac{\tau''}{\rho} = \frac{\lambda}{6\pi}\sqrt{\frac{(s-1)g\ d_b}{(\theta_o-0.047)}}\ \frac{(2h_o)}{d_b}\left[a_{br} - a_{bi} - \frac{1.2(kD)}{D}\sqrt{(\theta_o-0.047)(s-1)g\ d_b^3}\right] \tag{61}$$

where without loss of generality m is assumed to be zero. The temperature effect on the form drag is clearly shown in Eq. (61). The decrease in temperature stretches the dunes and reduces the migration velocity and the amplitude of the bed forms. Then from Eq. (61), these effects decrease the form roughness of the bed.

To check the validity of Eq. (61), field data from the Missouri River and the Rio Grande (see Table 1) are employed to determine the correction factor λ. The quantities τ'', h_o, kD, D and θ_o are obtained from the field data, and the values of a_{br}, a_{bi}, and d_b are evaluated from the stability theory. The results are plotted in Fig. 7 to relate λ and T. It is found that λ decreases with temperature and approaches unity at low temperatures. The reasons are:

(i) At high temperatures, the bed configuration is dunes that have approximately triangular profiles with long gentle upstream slopes and short steep downstream slopes causing large separation zones

in the flow. These profiles and large separation zones of dunes are not well simulated by the stability theory, which assumes a sinuous bed profile and small wave amplitude and separation zone. Therefore, the energy dissipation caused by dunes is expected to be larger than estimated from the theory. The correction factor accounts for this difference.

(ii) At low temperatures, the bed wave is smoothed out approaching a sinuous profile as described by Eq. (6). This enables the theory to simulate the flow field.

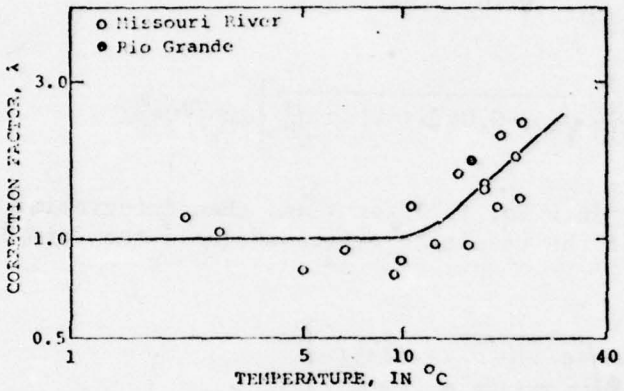

Figure 7.--Temperature effects on the resistance correction factor.

The scatter in Fig. 7 is mainly caused by fluctuations in the amplitudes of the bed waves. By using a more consistent method to analyze the bed forms, the scatter could be reduced.

2. Design Principles

Eq. (61) involves properties of the bed forms and is not practical for design purposes. A more generalized method is thus developed. Eq. (61) is rearranged in the form

$$\frac{\tau''}{\rho} = \left\{\frac{1}{3\pi}\left(\frac{d_b}{d_{50}}\right)^{\frac{1}{2}}\right\}\sqrt{\frac{(s-1)g\ d_{50}}{\theta'_o-0.047}}\left\{\lambda\ \frac{h_o}{d_b}\left[\frac{a_{br}}{V} - \frac{a_{bi}}{V}\right.\right.$$

$$\left.\left. - \frac{1.2(kD)}{VD}\sqrt{(\theta_o-0.047)(s-1)g\ d_b^3}\right]\right\} V = \left\{f\right\}\sqrt{\frac{(s-1)g\ d_{50}}{\theta'_o-0.047}}\left\{c\right\}\ V \qquad (62)$$

where $\theta'_o = \dfrac{\tau'}{(s-1)g\ d_{50}} + 0.1\ S_o$, and S_o is the mean bed slope. The coefficient c is related to the disturbed flow characteristics and f is a function of size distribution and flow conditions. In Eq. (62),

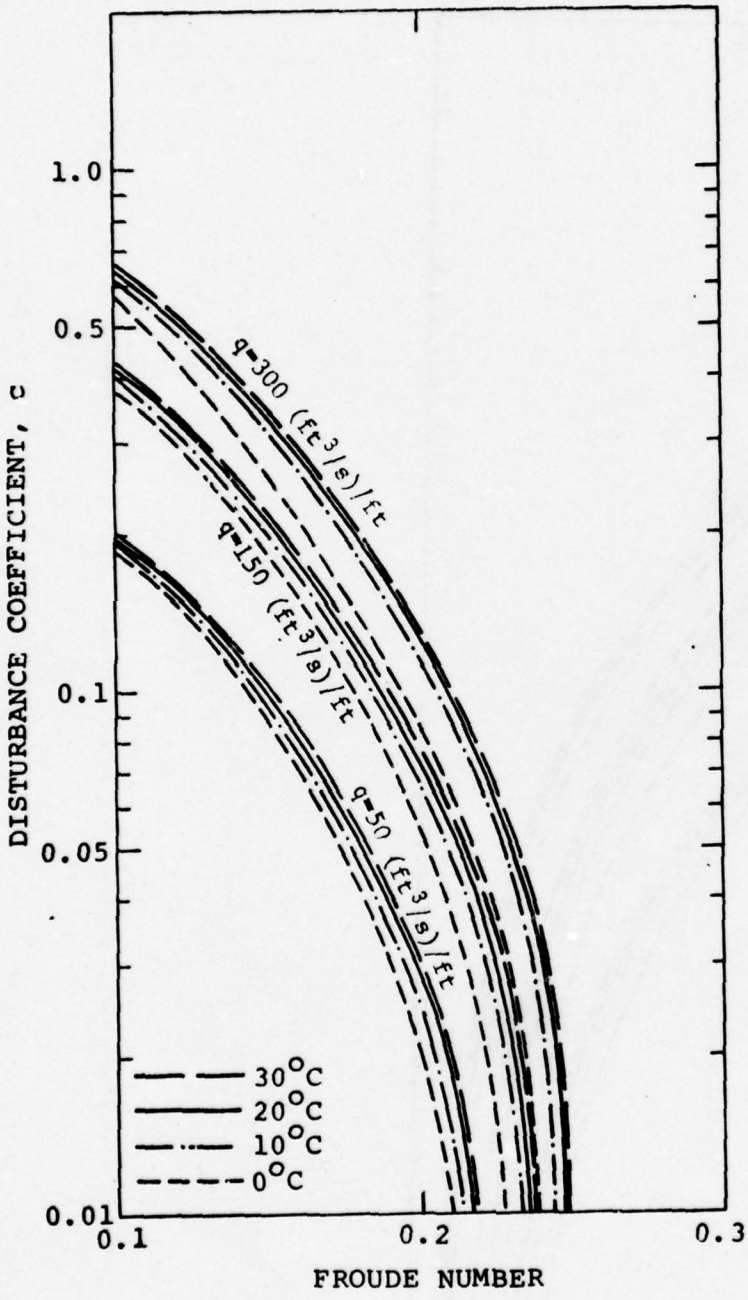

Figure 8a.--Relation for disturbance coefficient (d_{50} = 0.2 mm, S = 0.00005)

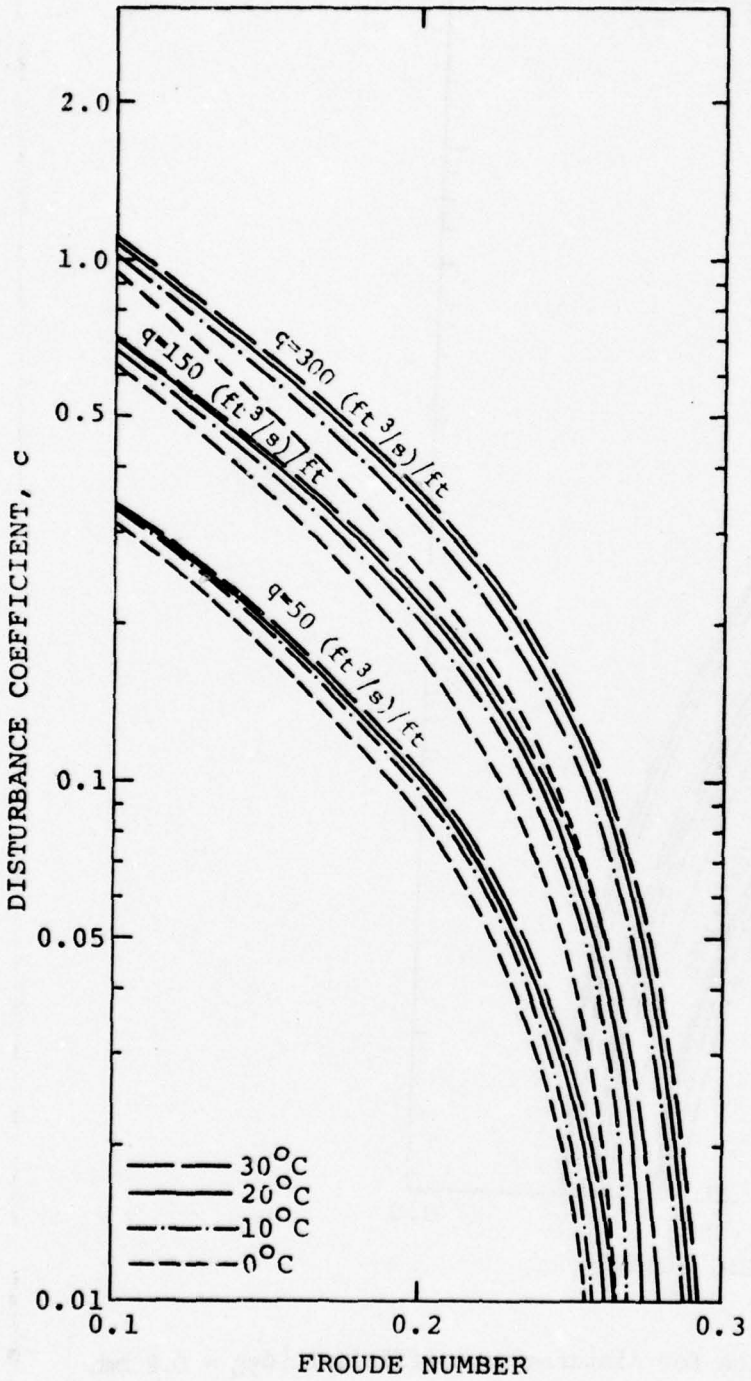

Figure 8b.--Relation for disturbance coefficient (d_{50} = 0.2 mm, S = 0.000075)

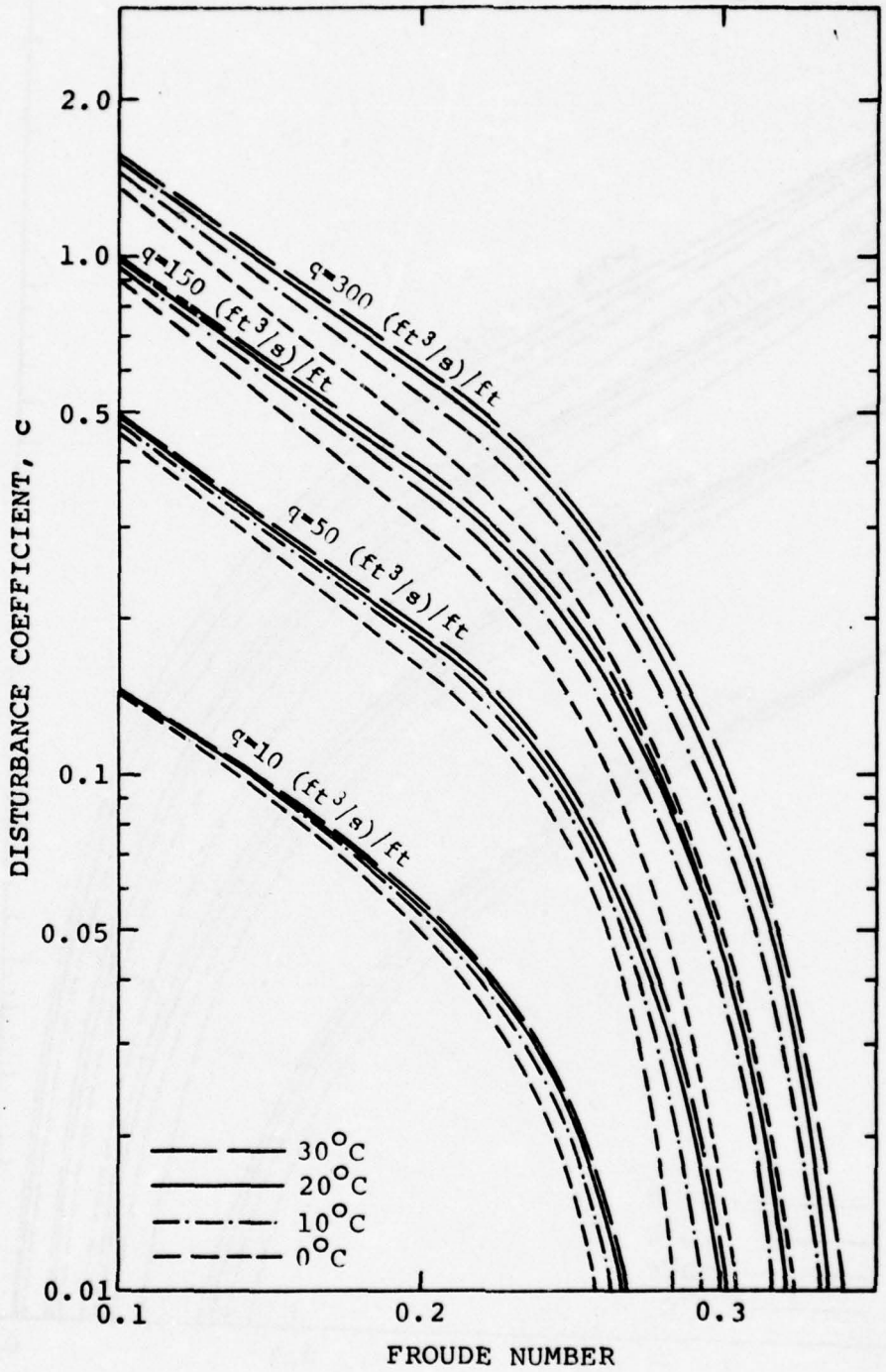

Figure 8c.--Relation for disturbance coefficient (d_{50} = 0.2 mm, S = 0.0001)

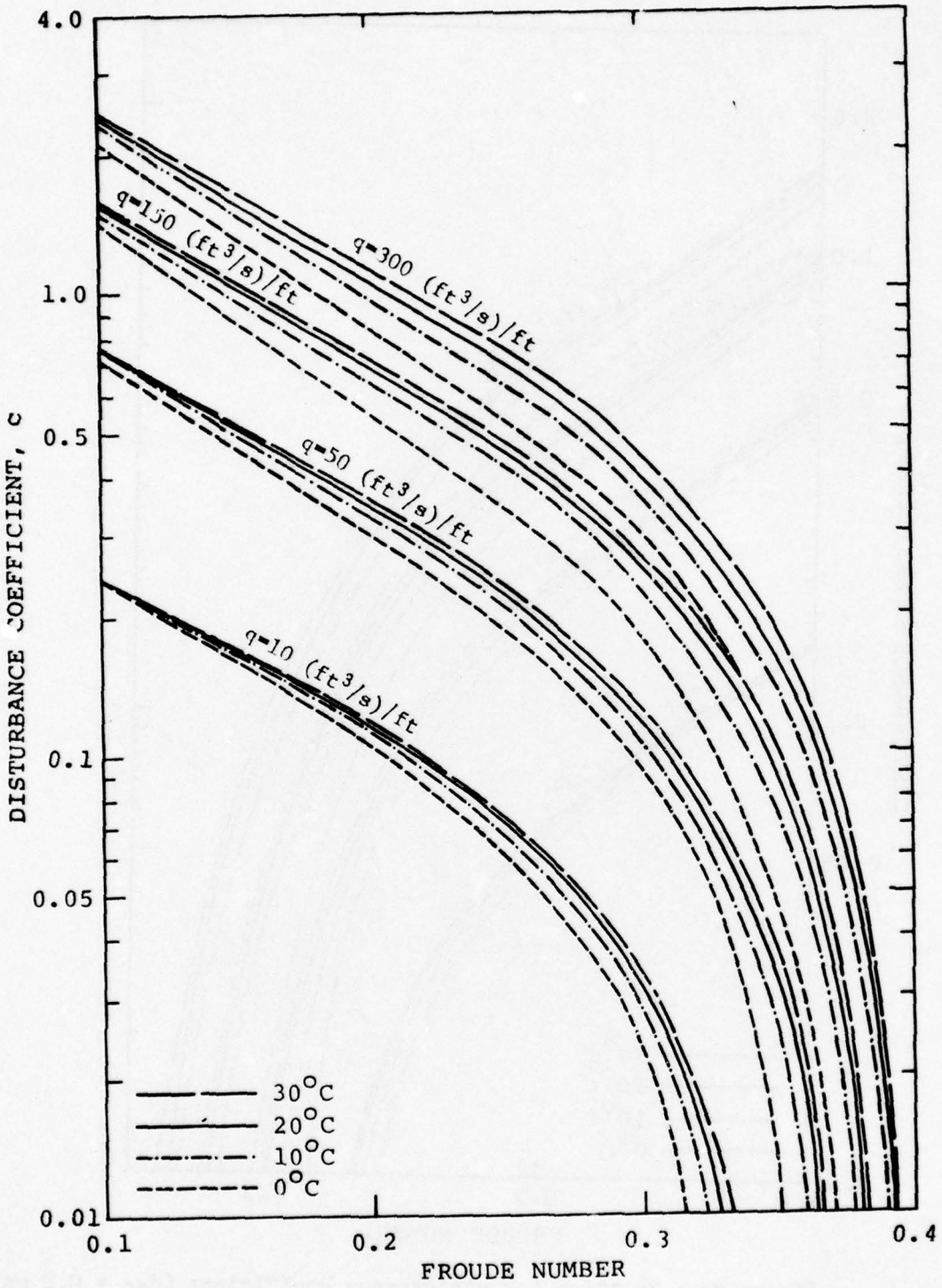

Figure 8d.--Relation for disturbance coefficient (d_{50} = 0.2 mm, S = 0.00015)

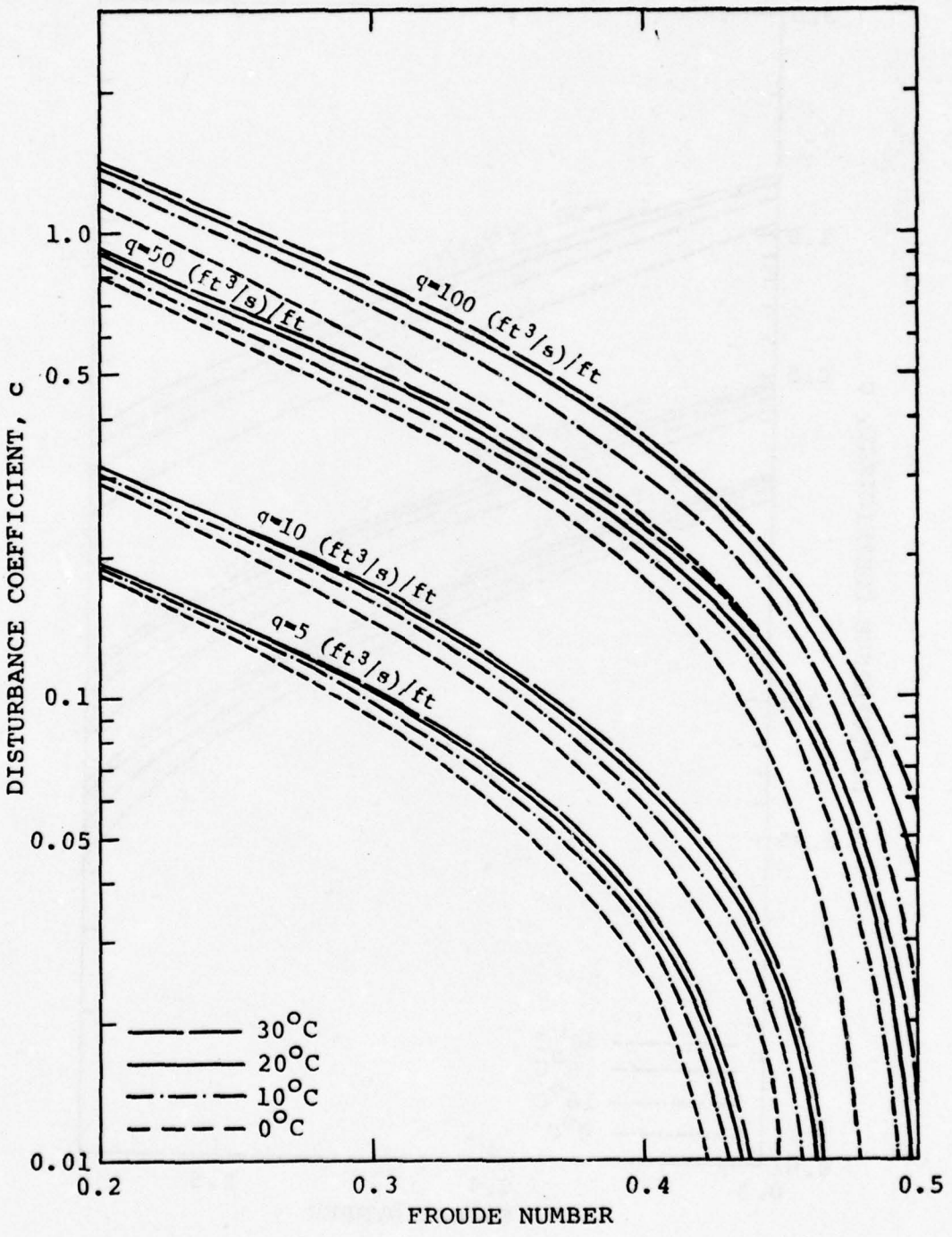

Figure 8e.--Relation for disturbance coefficient (d_{50} = 0.2 mm, S = 0.0003)

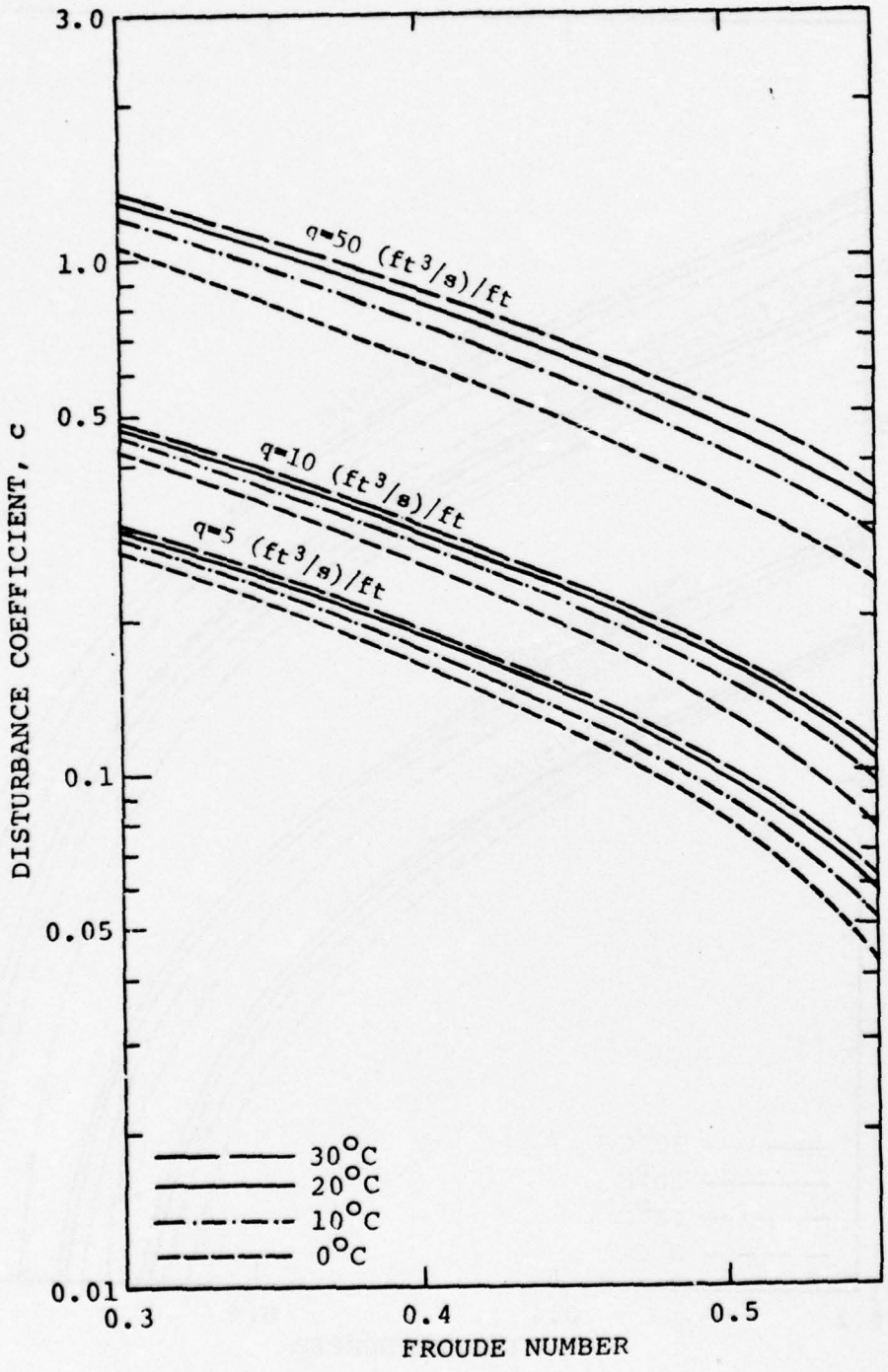

Figure 8f.--Relation for disturbance coefficient (d_{50} = 0.2 mm, S = 0.0006)

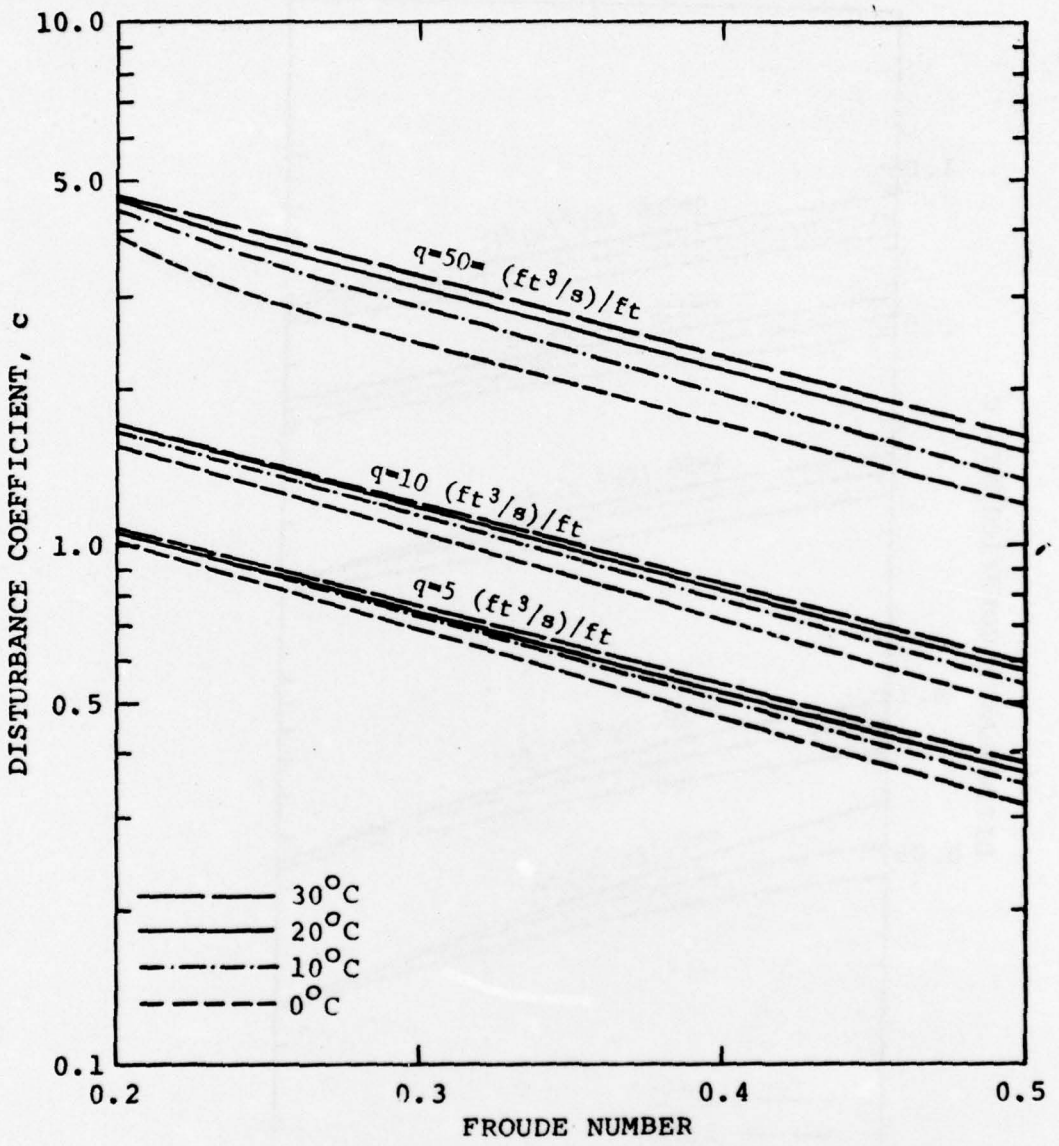

Figure 8g.--Relation for disturbance coefficient (d_{50} = 0.2 mm, S = 0.0012)

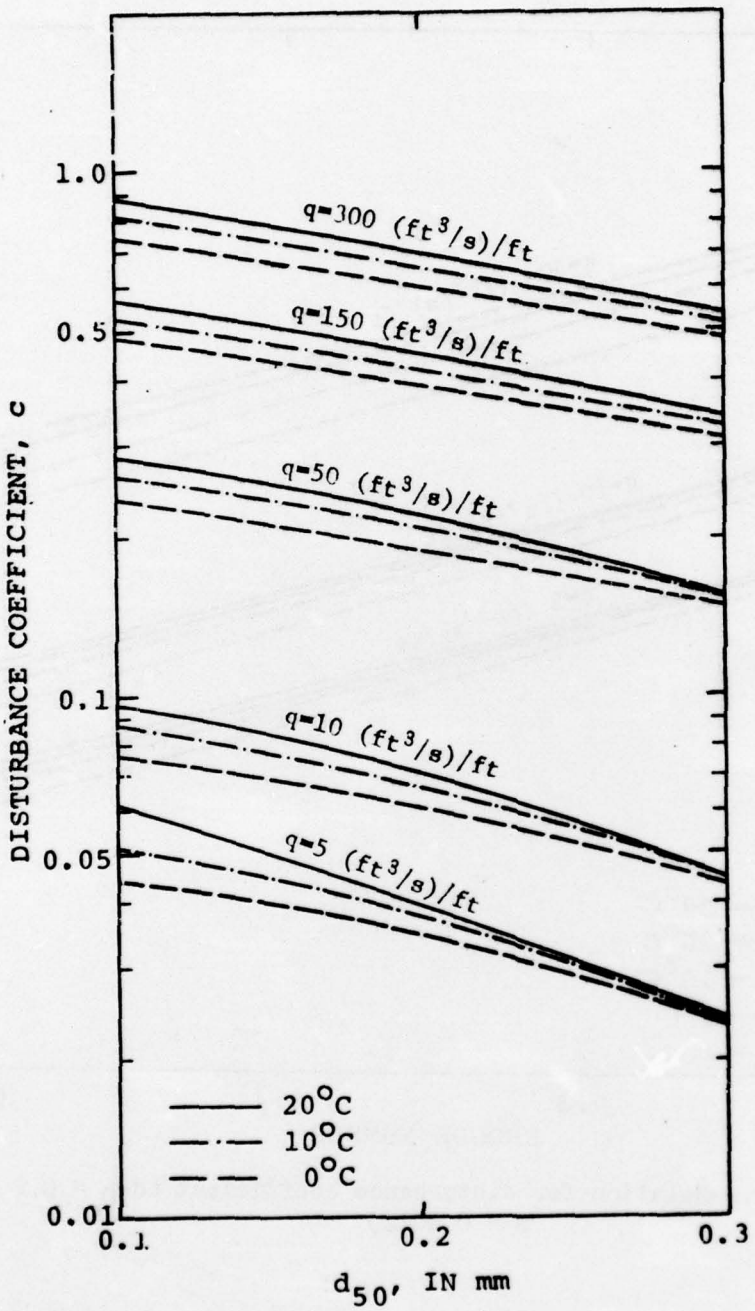

Figure 9.--Sediment grain size adjustment for the coefficients from fig. 8.

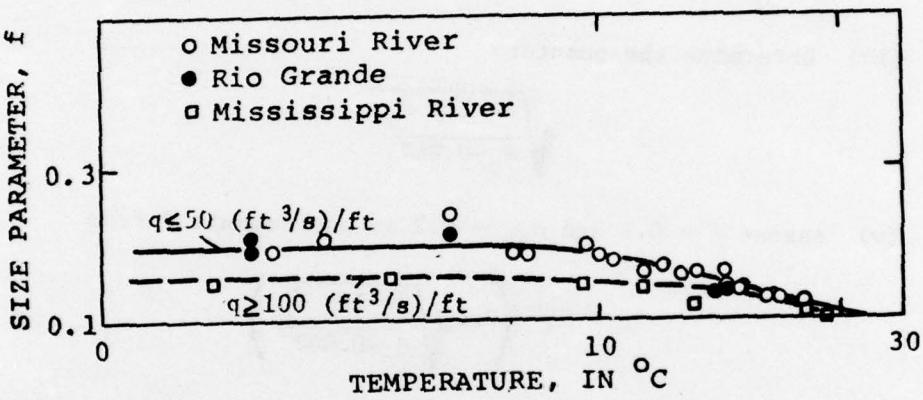

Figure 10.--Empirical relation of size parameter.

the value $\lambda h_o/d_b$ can not be evaluated from stability theory. An alternate method is used for determination of c as follows:

(i) Given q, F, T, d_{50}, σ, and S_o, compute U'_* from Fig. 2.

(ii) Compute d_b based on the Sec. 2-(3).

(iii) Compute the shear velocity

$$U''^2_* = gDS_o - (U'^2_*)$$

(iv) Determine the quantity

$$\sqrt{\frac{(s-1)g\ d_b}{\theta_o - 0.047}}$$

(v) Assume f = 0.1 and d_{50} = 0.2 mm and compute c from

$$c = U''^2_* \Big/ \left(0.1\sqrt{\frac{(s-1)g\ d_b}{\theta_o - 0.047}}\right)$$

The calculated results of c are plotted on Fig. 8 as functions of q, F, T, σ and S_o. These figures are employed to determine c for the following conditions:

(i) q = 5 - 300 $(ft^3/s)/ft$,

(ii) S_o = 0.00005 - 0.0012,

(iii) d_{50} = 0.2 mm,

and (iv) T = 0 - 30° Celsius.

The values of c decrease with temperature, indicating that the decrease in water temperature will reduce the degree of flow disturbance by bed forms.

To determine the effect of particle size on values of c, families of curves defining c as a function of particle size, unit water discharge, and water temperature can be constructed for constant values of slope and Froude number. A set of curves for slope S = 0.00015 and Froude number F = 0.25 is shown in Fig. 9. The relative positions of the curves are not changed much for other values of slope and Froude number, so the curves in Fig. 9 can be used to adjust for bed particle sizes from 0.1 to 0.3 mm the values of c determined from Fig 8, which

which are given for d_{50} = 0.2 mm. An example of the adjustment is given in the appendix.

The coefficient f is treated as an empirical coefficient. Its values are obtained from Eq. (62) and Fig. 8 by determining the other quantities in Eq. (62) for given field flow data and then computing f from Eq. (62). Those field data from the Mississippi River, the Missouri River and the Rio Grande Conveyance Channel, which show significant temperature effects, are utilized to develop the empirical relation for f. The values of f are tabulated in Table 1 and are plotted on Fig. 10 as functions of water temperatures and unit-width flow discharges. The values of f increase with decrease in temperature because of the coarsening of bed load. Figs. 2, 8, 9, and 10 are employed to determine resistance to flow with characteristics close to the transition zone. A detail example and step-by-step procedure are presented in the appendix to determine flow velocity and depth for given unit-width discharge q, water surface slope S, temperature T and median size of bed material d_{50}.

An example of variation in the flow characteristics with temperature evaluated from the design curves is shown in Fig. 11. It indicates that the flow depth decreases with temperature for a given unit-width flow discharge because of the change in resistance to flow with temperature.

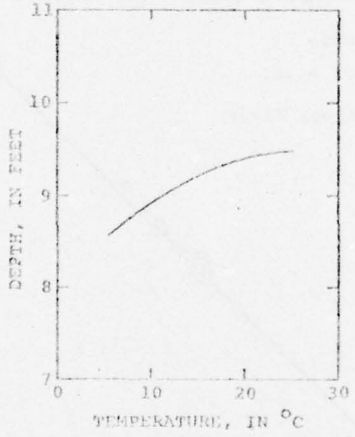

Figure 11.--Temperature effects on flow resistance (q = 40 cfs/ft, S = 0.002, d_{50} = 0.22 mm, σ = 1.3).

3. Application Field Data

To verify the proposed design curves, Figs. 2, 8, 9, and 10 are employed to reproduce the field data listed in Table 1. The required information is the quantities q, S_o, T, d_{50}, and d_{65}. The calculated results are the flow depth D and the velocity V. The calculated depths show good agreement with the measured values as shown in Fig. 12.

4. Limitation of Design Curves

The design curves for evaluating flow resistance have several limitations:

(i) The design curves are developed from linear stability theory. The basic assumption of this theory is that $h_o/D<<1$. Therefore, for small flow depth, say $D<4$ ft, the design curves are not applicable.

(ii) The design curves are only applicable to flow regimes close to the transition zone. It is suggested that the stream power

$$\tau V = \rho g q S$$

should be greater than about 0.27 (lbs/ft)/s to apply the design curves.

(iii) The design curves cover the range of sediment grain sizes 0.1 - 0.3 mm, temperatures 0 - 30° Celsius, unit-width flow discharges 5 - 300 $(ft^3/s)/ft$, and slope 0.00005 - 0.0012. Extension of the curves outside these ranges is not recommended.

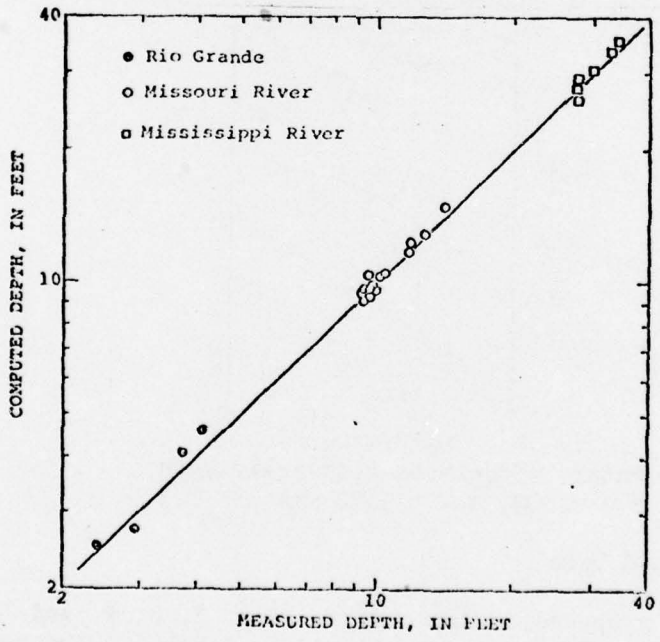

Figure 12.--Comparison between measured and calculated depths.

SUMMARY AND CONCLUSION

When the flow regime is close to the transition zone, the temperature effects on the flow characteristics, sediment transport rate, bed configuration and its resistance to flow become quite significant. It is found in many cases that a decrease in temperature removes the dunes from the sand bed, decreases flow resistance and depth, and increases flow velocity and sediment transport rate.

Stability theory that includes the effect of temperature on the flow characteristics in alluvial channels was developed by Engelund and Fredsøe (1974). The theory shows qualitatively the temperature effects on the flow field. To quantitatively predict temperature effects, the idea of disturbed flow on bed forms developed from the stability theory is introduced to describe the form roughness. An equation relating the form drag to the disturbed shear stress is thus derived. This relation yields suitable form drag for low temperatures where the bed is smooth but not for high temperatures with a dune bed. A correction factor introduced in the equation indicates that the form drag is about twice as much as that evaluated from the stability theory.

A set of design curves is developed from the stability theory to estimate the flow resistance in terms of evaluation of flow depth and velocity including temperature as a major factor. The initial data required to apply the procedure are the unit water discharge, water temperature, energy slope, and particle size distribution of bed material.

REFERENCES

Anderson, A. G., 1953, The characteristics of sediment waves formed by flow in open channels: Proc. Third Midwestern Conf. on Fluid Mech., Univ. of Minnesota.

Colby, B. R., and Scott, C. H., 1965, Effects of water temperature on the discharge of bed material: U.S. Geol. Survey Prof. Paper 462-G, 25 p.

Culbertson, J. K., Scott, C. H., and Bennett, J. P., 1972, Summary of alluvial-channel data from Rio Grande Conveyance Channel, New Mexico, 1965-1969: U.S. Geol. Survey Prof. Paper 562-J, 49 p.

Engelund, Frank, 1970, Instability of erodible beds: Jour. of Fluid Mech., v. 42, part 2, p. 225-244.

Engelund, Frank, 1973, Steady transport of moderately graded sediment: Prog. Rep. 29, Inst. Hydrodynamics and Hydraulic Engineering, Tech. Univ. of Denmark, p. 3-12.

Engelund, Frank, and Fredsøe, Jorgen, 1974, Transition from dunes to plane bed in alluvial channels: Series Paper No. 4, Inst. of Hydrodynamics and Hydraulic Engineering, Tech. Univ. of Denmark, Lyngby, Denmark, 56 p.

Engelund, Frank, and Hansen, Eggert, 1966, Investigations of flow in alluvial streams: Octa Polytechnica Scandinavica, 100 p.

Exner, F. M., 1925, Uber die wechselwirkung zwischen wasser und geschiete in flussen: Sitzenberichte der Academie der Wissenchaften, Wien, Heff 3-4.

Gilbert, G. K., 1914, The transportation of debris by running water: U.S. Geol. Survey Prof. Paper 86, 263 p.

Gradowczyk, M. H., 1968, Wave propagation and boundary instability in erodible-bed channels: Jour. Fluid Mechanics, v. 33, pt. 1, p. 93-112.

Hayashi, Taizo, 1970, Formation of dunes and antidunes in open-channels: Proc. Amer. Soc. of Civil Engineers, v. 96, no. HY2, p. 357-366.

Hinze, J. O., 1959, Turbulence: McGraw-Hill Book Co., Inc., New York, 586 p.

Jordan, P. R., 1965, Fluvial sediment of the Mississippi River at St. Louis, Missouri: U.S. Geol. Survey Water-Supply Paper 1802, 89 p.

Kennedy, J. F., 1961, Stationary waves and antidunes in alluvial channels: California Institute of Tech., Pasadena, California, report no. KH-R-2, 146 p.

Kennedy, J. F., 1963, The mechanics of dunes and antidunes in erodible-bed channels: Jour. of Fluid Mech., v. 16, part 4, p. 521-544.

Kennedy, J. F., 1964, The formation of sediment ripples in closed rectangular conduits and in the desert: Jour. Geophys. Res., v. 69, no. 8, p. 1517-1524.

Kennedy, J. F., 1969, The formation of sediment ripples, dunes, and antidunes: Annual Review of Fluid Mechanics, v. 1, p. 147-168.

Kennedy, J. F., and Falcon, M., 1965, Wave-generated sediment ripples: School of Engineering Report no. 86, Mass. Inst. of Tech., Boston, 55 p.

Pierce, R. C., 1916, The measurement of silt-laden streams: U.S. Geol. Survey Water-Supply Paper 400-C, p. 39-51.

Polya, G., 1937, Zur kinematik der Geschiebebewegung, Verlag Rascher and Co., Zurich, 21 p.

Reynolds, A. J., 1965, Waves on the erodible bed of an open-channel: Jour. of Fluid Mech., v. 22, part 1, p. 113-133.

Smith, J. D., 1970, Stability of a sand bed subjected to a shear flow of low Froude number: Jour. of Geophys. Research, v. 75, no. 30, p. 5928-5940.

U.S. Army Corps of Engineers, 1969, Missouri River channel regime studies: M.R.D. Sediment Series no. 13B, U.S. Army Engineer Div., Missouri River, Corps of Engineers, Omaha, Nebraska, 13 p., 63 plates.

Vanoni, V. A., and Brooks, N. H., 1957, Laboratory studies of roughness and suspended load of alluvial streams: M.R.D. Sediment Series no. 11, U.S. Army Engineer Division, Missouri River, Corp of Engineers, Omaha, Nebraska, 121 p.

APPENDIX

1. Numerical Example

A detailed numerical example is presented to show the application of design curves Figs. 2, 8, 9, and 10 to determine the flow resistance. The given information is

(i) q = 40 $(ft^3/s)/ft$,

(ii) T = 5°C,

(iii) S_o = 0.0002,

(iv) d_{50} = 0.22 mm,

and (v) d_{65} = 0.25 mm,

The following table shows the calculation procedure with explanations:

F	V	$U2$	$U3$	$U1$	U_*'	D'	c	f	P_o	$U_*''^2$	D''	D	q_c
(1)	(2)	(3)	(4)	(5)	(6)	(7)	(8)	(9)	(10)	(11)	(12)	(13)	(14)
0.275	4.59	1996	9.2×10^8	28.5	0.161	4.03	0.197	.140	.247	.0313	4.86	8.89	40.80
0.29	4.75	2068	1.02×10^9	28.5	0.166	4.28	0.164	.140	.239	.0260	4.04	8.32	39.52

Col. (1): Assume a Froude number.

Col. (2): Compute the mean flow velocity from $V = F^{2/3}(gq)^{1/2}$.

Col. (3): Compute $U2 = V/\sqrt{gd_{65}S_o}$.

Col. (4): Compute $U3 = V^3/g\nu S_o$.

Col. (5): Find $U1$ from Fig. 2 for the given $U2$ and $U3$.

Col. (6): Compute the effective shear velocity from $U_*' = V/U1$.

Col. (7): The depth due to grain roughness $D' = U_*'^2/gS_o$.

Col. (8): Determine the disturbance coefficient from the following procedure:

(i) Discharge and slope adjustment:

(a) Choose from Fig. 8 the suitable design curves which bracket the given q and S_o. In this example, Figs. 8d and 8e are chosen.

(b) From Fig. 8d, $c = 0.145$ for $q = 50$ $(ft^3/s)/ft$, $F = 0.275$, $T = 5°C$ and $S_o \approx 0.00015$; and $c = 0.044$ for $q = 10$ $(ft^3/s)/ft$, $F = 0.275$, $T = 5°C$ and $S_o = 0.00015$. Then by interpolating on a logarithmic graph of q versus c, we can find $c = 0.123$ for $q = 40$ $(ft^3/s)/ft$, $F = 0.275$, $T = 5°C$, and $S = 0.00015$.

(c) Using the same procedure as (b), we can find $c = 0.445$ for $q = 40$ $(ft^3/s)/ft$, $F = 0.275$, $T = 5°C$, and $S = 0.0003$ from Fig. 8e.

(d) By interpolating on a logarithmic graph of c versus S, we can find that $c = 0.210$ for $q = 40$ $(ft^3/s)/ft$, $F = 0.275$, $T = 5°C$, $S = 0.0002$ and $d_{50} = 0.20$ mm.

(ii) Sediment grain size adjustment

(a) Using Fig. 9, find locations of c for ($q = 50$ $(ft^3/s)/ft$, $d_{50} = 0.2$ mm) and ($q = 50$ $(ft^3/s)/ft$, $d_{50} = 0.22$ mm given) and measure the vertical distance between them. In this example, the distance $d_c \approx -0.2$ cm (because c for 0.22 mm is below that for 0.20 mm).

(b) Measure the vertical distance between locations of for $d_m = 0.2$ mm and discharges which bracket the given discharge from Fig. 9. In this example, the distance $d_{c1} = 3.72$ cm.

(c) Measure the distance between locations of c for discharges which bracket the given discharge and the Froude number assumed at step 1 from the figure with slope closest to the given slope. In this example, the distance $d_{c2} = 3.92$ cm from Fig. 8d.

(d) Compute the correction distance, d_c', = 3.72.

$$d_c' = (d_c)(d_{c2})/(d_{c1})$$

$$= (-0.2)(3.92)/(3.72) = -0.21 \text{ cm.}$$

(e) Locate the value of c from (i) on a logarithmic graph with scale the same as Fig. 9 and add distance d'_c to obtain the value of $c = 0.197$ for $q = 40$ (ft^3/s)/ft, $S = 0.0002$, $F = 0.275$, $T = 50$C, and $d_m = 0.22$ mm.

Col. (9): Find f from Figure 10 for given q and T.

Col. (10): Compute the value of P_o from

$$P_o = \sqrt{\frac{(s-1)g\ d_{50}}{\theta_o - 0.047}}$$

where

$$\theta_o = \frac{(U'_*)^2}{(s-1)g\ d_{50}} + 0.1\ S_o$$

Col. (11): Compute the shear velocity from Eq. (62), i.e.,

$$U''^{\,2}_* = fP_o cV$$

Col. (12): Compute the depth due to form roughness from

$$D'' = U''^{\,2}_*/gS_o$$

Col. (13): The total depth equals

$$D = D' + D''$$

Col. (14): The calculated discharge is then

$$q_c = VD$$

If q_c is different from the given flow discharge, Steps (1) through (14) are repeated until the calculated discharges bracket the given flow discharge. The flow depth is then obtained based on linear interpolation with the discharge. In general, the increase in the Froude number decreases the calculated discharge. After interpolation, the flow depth is found to be 8.55 ft.

2. Table 1

Table 1 Summary of Field Data

Source	Date	T (°C)	V (fps)	D (ft)	Dune L (ft)	Dune H (ft)	S (ft/1000 ft)	d_{50} (mm)	d_{65} (mm)	f	η
Missouri River[1]	9/8/66	21.6	4.48	10.11	210	3.3	.15	.21	.23	.110	1.80
	9/13/66	22.8	4.51	10.33	205	2.9	.15	.21	.23	.110	2.28
	9/19/66	17.8	4.58	9.84	350	3.3	.15	.21	.23	.117	1.41
	9/26/66	17.8	4.58	10.00	335	3.4	.15	.21	.23	.116	1.46
	10/3/66	14.5	4.72	9.58	420	2.6	.15	.21	.23	.122	1.62
	10/10/66	15.6	5.00	9.30	370	2.8	.15	.21	.23	.123	.96
	10/17/66	9.4	5.36	9.35	450	2.7	.15	.21	.23	.141	.76
	10/24/66	10.0	5.11	9.14	395	2.5	.15	.21	.23	.133	.88
	11/7/66	6.7	5.12	9.24	570	2.4	.15	.21	.23	.136	.94
	8/21/67	22.2	4.59	10.13	250	3.8	.15	.21	.23	.112	1.32
	9/25/67	17.7	5.19	9.56	370	4.7	.15	.21	.23	.125	.58
	10/24/67	12.3	5.01	9.82	315	3.8	.15	.21	.23	.124	.96
	11/22/67	5.0	5.49	9.11	170	1.9	.15	.21	.23	.161	.80
	8/6/68	25.6	4.23	11.70			.15	.21	.23	.109	
	9/10/68	18.9	4.54	10.15	229	3.2	.15	.21	.23	.114	1.23
	10/7/68	13.3	5.34	9.64	315	2.8	.15	.21	.23	.129	1.27
	12/2/68	2.2	5.08	9.67	2412	3.0	.15	.21	.23	.137	1.16
	9/23/69	19.5	5.44	14.04	224	3.4	.15	.21	.23	.117	2.04
	10/14/69	10.6	5.66	12.65	308	3.1	.15	.21	.23	.131	1.28
	11/4/69	7.2	5.52	11.79	332	2.7	.15	.21	.23	.134	1.37
	12/1/69	2.8	5.29	10.08	1120	2.3	.15	.21	.23	.144	1.08
Mississippi River[2]	2/18/52	3.9	4.24	27.90			.0544	.19	.21	.122	
	4/27/53	12.2	4.42	33.00			.0589	.19	.21	.117	
	6/13/53	26.7	4.00	30.10			.0632	.24	.27	.102	
	7/20/53	28.9	3.54	27.90			.0603	.23	.25	.100	
	8/10/53	26.1	3.61	27.60			.0661	.22	.24	.105	
	6/7/54	19.4	4.96	34.20			.0691	.23	.25	.113	
	2/24/55	1.7	5.11	34.00			.0720	.25	.27	.120	
Rio Grande[3]	6/10/65	17.0	2.67	2.76	50	2.8	.64	.23	.25	.110	1.72
	11/29/65	5.0	4.98	3.69			.66	.18	.20	.149	
	12/14/66	2.0	4.05	2.48			.70	.20	.22	.138	
	12/13/66	2.0	4.66	2.76			.71	.20	.22	.147	
	6/11/69	18.0	3.62	5.11			.69	.28	.31	.115	

[1] Data are from Corps of Engineers (1969) and personal communication from Mr. Warren Mellema, Corps of Engineers, Omaha District.
[2] Data are from Jordan (1965)
[3] Data are from Culbertson and others (1972).